Check for updates

ARTICLE

Cellular and Molecular Biology

Evolution of cisplatin resistance through coordinated metabolic reprogramming of the cellular reductive state

Wangie Yu[1], Yunyun Chen[2], Nagireddy Putluri[3], Abdullah Osman[2], Cristian Coarfa[3,4,5], Vasanta Putluri[6], Abu H. M. Kamal[6], Jennifer Kay Asmussen[7], Panagiotis Katsonis[7], Jeffrey N. Myers[2], Stephen Y. Lai[2,8,9], Wuhao Lu[1], Clifford C. Stephan[10,11], Reid T. Powell[10,11], Faye M. Johnson[12], Heath D. Skinner[13], Jawad Kazi[1], Kazi Mokim Ahmed[1], Linghao Hu[14], Addison Threet[14], Matthew D. Meyer[15], James A. Bankson[16], Tony Wang[1], Jack Davis[1], Kirby R. Parker[1], Madison A. Harris[1], Mokryun L. Baek[3,5,17,18], Gloria V. Echeverria[3,5,17,18], Xiaoli Qi[19], Jin Wang[3,19], Andy I. Frederick[20], Alex J. Walsh[14], Olivier Lichtarge[7,19,21,22,23,24], Mitchell J. Frederick[1✉] and Vlad C. Sandulache[1,3,25✉]

BACKGROUND: Cisplatin (CDDP) is a mainstay treatment for advanced head and neck squamous cell carcinomas (HNSCC) despite a high frequency of innate and acquired resistance. We hypothesised that tumours acquire CDDP resistance through an enhanced reductive state dependent on metabolic rewiring.
METHODS: To validate this model and understand how an adaptive metabolic programme might be imprinted, we performed an integrated analysis of CDDP-resistant HNSCC clones from multiple genomic backgrounds by whole-exome sequencing, RNA-seq, mass spectrometry, steady state and flux metabolomics.
RESULTS: Inactivating KEAP1 mutations or reductions in KEAP1 RNA correlated with Nrf2 activation in CDDP-resistant cells, which functionally contributed to resistance. Proteomics identified elevation of downstream Nrf2 targets and the enrichment of enzymes involved in generation of biomass and reducing equivalents, metabolism of glucose, glutathione, NAD(P), and oxoacids. This was accompanied by biochemical and metabolic evidence of an enhanced reductive state dependent on coordinated glucose and glutamine catabolism, associated with reduced energy production and proliferation, despite normal mitochondrial structure and function.
CONCLUSIONS: Our analysis identified coordinated metabolic changes associated with CDDP resistance that may provide new therapeutic avenues through targeting of these convergent pathways.

INTRODUCTION

For more than three decades platinum-based chemotherapy has been a frontline systemic treatment for advanced squamous cell carcinomas of the head and neck (HNSCC), lung (LUSCC) and other solid tumours, despite a high prevalence of innate and acquired resistance among patients with these cancer types [1–10]. A more precise understanding of how tumours survive the stress of platinum agents or evolve into therapy-resistant populations is paramount to overcoming treatment failure and maximising disease control. Enhanced DNA repair, altered activation of

[1]Bobby R. Alford Department of Otolaryngology Head and Neck Surgery, Baylor College of Medicine, Houston, TX, USA. [2]Department of Head and Neck Surgery, University of Texas MD Anderson Cancer Center, Houston, TX, USA. [3]Department of Molecular and Cellular Biology, Baylor College of Medicine, Houston, TX, USA. [4]Center for Precision Environmental Health, Baylor College of Medicine, Houston, TX, USA. [5]Dan L. Duncan Cancer Center, Baylor College of Medicine, Houston, TX, USA. [6]Advanced Technology core, Dan Duncan Cancer Center, Baylor College of Medicine, Houston, TX, USA. [7]Department of Molecular and Human Genetics, Baylor College of Medicine, Houston, TX, USA. [8]Department of Molecular and Cellular Oncology, University of Texas MD Anderson Cancer Center, Houston, TX, USA. [9]Department of Radiation Oncology, University of Texas MD Anderson Cancer Center, Houston, TX, USA. [10]Institute of Biosciences and Technology, Texas A&M Health Science Center, Houston, TX, USA. [11]Department of Translational Medical Sciences, School of Medicine, Texas A&M University, Houston, TX, USA. [12]Department of Thoracic Head and Neck Medical Oncology, Division of Cancer Medicine, University of Texas MD Anderson Cancer Center, Houston, TX, USA. [13]Department of Radiation Oncology, UPMC Hillman Cancer Center, Pittsburgh, PA, USA. [14]Biomedical Engineering, Texas A&M University, College Station, TX, USA. [15]Shared Equipment Authority, Rice University, Houston, TX, USA. [16]Department of Imaging Physics, The University of Texas MD Anderson Cancer Center, Houston, TX, USA. [17]Lester and Sue Smith Breast Center, Baylor College of Medicine, Houston, TX, USA. [18]Department of Medicine, Baylor College of Medicine, Houston, TX, USA. [19]Department of Pharmacology and Chemical Biology, Baylor College of Medicine, Houston, TX, USA. [20]School of Electrical and Computer Engineering Undergraduate Department, Cornell University, NY, USA. [21]Department of Biochemistry & Molecular Biology, Baylor College of Medicine, One Baylor Plaza, Houston, TX, USA. [22]Program in Quantitative and Computational Biosciences, Baylor College of Medicine, One Baylor Plaza, Houston, TX, USA. [23]Program in Integrative Molecular and Biomedical Sciences, Baylor College of Medicine, One Baylor Plaza, Houston, TX, USA. [24]Computational and Integrative Biomedical Research Center, Baylor College of Medicine, One Baylor Plaza, Houston, TX, USA. [25]Center for Translational Research on Inflammatory Diseases, Michael E. DeBakey Veterans Affairs Medical Center, Houston, TX, USA. ✉email: Mitchell.Frederick@bcm.edu; vlad.sandulache@bcm.edu

programmed cell death cascades and differential transport of platinum agents have all been linked to cisplatin (CDDP) response and development of resistance [5, 10–13]. We and others have proposed a fourth mechanism whereby reactive intracellular CDDP becomes neutralised before it can damage vital macromolecules like DNA. Despite the clear metabolic requirements of each of these processes and the need for wholesale metabolic reprogramming, coordinated at a transcriptional level, the critical components of this metabolic adaptation remain unclear [2–5, 7–9, 11, 12, 14–16]. A better understanding of how transcriptomic rewiring carefully meets the metabolic needs generated by genotoxic stress will likely identify novel dependencies that could be targetable by either direct metabolic blockade, drugs inhibiting tyrosine or receptor tyrosine kinases (i.e., TKi's or RTKi's), or miRNA-based inhibition of protein signalling. Moreover, since metabolic adaptation to stress generates distinct immunogenic cues, targeting tumour metabolism may simultaneously enhance the effectiveness of current immune therapy strategies [17, 18].

We have previously found that HNSCC and other tumours respond to oxidative stress through temporary shifts in carbon flux designed to ameliorate the burden on intracellular reducing equivalent reserves, even at the expense of energy generation [19]. In this study, we sought first, to determine whether the acquisition of CDDP resistance in a conditioned exposure model is associated with permanent shifts in carbon flux and second, to identify the potential genomic and transcriptomic mechanisms which support and underly this shift.

MATERIALS AND METHODS
Cells
HN30, HN31 and PCI13 are HNSCC tumour lines previously described and obtained from an established cell line bank in the laboratory of Dr. Jeffrey N. Myers. HN30 (TP53 wild type) and HN31 (TP53 mut) were originally derived from a primary and metastatic site, respectively, of the same patient [20]. We previously described an acquired CDDP resistance model developed in HN30 [9], which we extended to HN31 and PCI13 (Supplementary Table S1; Supplementary Materials and Methods).

Genomic, transcriptomic and proteomic analysis
Detailed analysis of genomic and transcriptomic data along with gene data preparation and gene set enrichment algorithms are summarised in Supplementary Materials and Methods [18, 21]. Briefly, DNA was extracted from cell lines with the DNeasy Tissue kit (Qiagen) and analysed through the Baylor College of Medicine Genomic and RNA Profiling Core (GARP) where size-selected DNA was captured using the Human All Exon v6 panel and prepared libraries and 'subjected to next-generation sequencing on an Illumina NovaSeq 6000 instrument with an average of 200 million reads per sample. Total RNA from logarithmic phase growth of samples, in biological triplicate, was prepared with the RNeasy Mini Kit (Qiagen) and analysed through GARP via next-generation sequencing which generated counts totalling more than 2 million reads per sample. Triplicate biological replicates from parental and CDDP-resistant cells were analysed using global profiling of proteins using an Orbitrap Elite Mass Spectrometer (Thermo-Fisher Scientific, Waltham, MA, USA).

Metabolic profiling
Steady-state and flux metabolomic experiments were performed as previously described and outlined in Supplementary Materials and Methods [8, 9]. Oxygen consumption rates (OCR) and extracellular acidification rates (ECAR) were assayed under basal conditions (25 mM D-glc, 1 mM pyruvate, 4 mM glutamine, 0% serum) using a Seahorse Bioscience XF24 Extracellular Flux Analyzer (Billerica, MA) [22]. Biolog metabolic assays were used to measure intrinsic mitochondrial activity in individual cell lines. Cells (30,000/well) were prepared according to the manufacturer's instructions (Biolog, Hayward, CA, USA) and permeabilized using saponin (30 µg/ml) prior to testing the effectiveness of individual substrates in generating a reducing effect. Real-time imaging of endogenous fluorescence for NAD(P)H and FAD was performed as

previously described (Supplementary Materials and Methods) [23–30]. HN30, HN30R4E1 and HN30R4F5 cells were seeded (~10^5) on 35-mm glass-bottom dishes 48 h before imaging; 4 µM CDDP was added to the HN30R4E1 and HN30R4F5 imaging dishes 24 h before imaging. Autofluorescence lifetime imaging was performed with a multiphoton fluorescence lifetime microscope (Marianas, 3i). The fluorescence lifetime decays at each pixel were fit to a two-component exponential decay, for the free and protein-bound NAD(P)H and FAD states [27, 31] and analysed using a semi-automated pipeline in CellProfiler [32].

Drug screening
Drug screening was performed by the Gulf Coast Consortia using previously described methods, focusing on established and validated compounds with known activity [33].

RESULTS
Generation of CDDP-resistant HNSCC cell lines
We previously described the generation of CDDP-resistant cell lines derived from HN30 [9]. To expand the genetic background of our experimental models, we also employed the same methodology to select for acquired CDDP resistance in HN31 (a naturally occurring TP53-mutant derived from a lymph node metastasis of the same patient as HN30) and in PCI13, another TP53-mutant cell line originating in the oral cavity (Supplementary Table S1). IC$_{50}$ values of resistant clones are approximately 20–100-fold greater than the previously described IC$_{50}$ values for CDDP in a panel of nearly 100 HNSCC cell lines [20, 34].

Somatic mutations in CDDP-resistant clones
The average number of new, detectable total mutations for CDDP-resistant clones from HN30, HN31, and PCI13 was 414, 858 and 790, respectively (Fig. 1a, Supplementary Table S2 and Supplementary Fig. 1A). We examined the degree to which novel mutations could be explained by exposure to CDDP, a known mutagen. All 12 CDDP-resistant clones had a significant mutation signature previously associated with CDDP treatment (Supplementary Table S3 and Supplementary Fig. 1B) which can be identified by an abundance of A[C > A]C, C[C > A]T, G[C > A]G, C[C > T]C, and C[C > T]T single base substitutions (SBS) [35]. Genes with the highest ratio of mutations/nucleotide included: LCE4A, KRTAP4-1, CLDN10, IGFBP2 and KRTAP9-1 (Supplementary Table S4). We ignored genes with known mapping issues (e.g., MUC3A) and focused on those with biological functions that could be linked to surviving genotoxic stress including DNA transcription (MESP1, MORF4L1), oxidative stress response (ADH4) and protein homeostasis (ATXN3). No enrichment was detected in mutational frequency of traditional tumour suppressors or oncogenes such as RAS, PIK3CA, NOTCH and TP53, nor in cancer drivers previously linked to HNSCC except for KEAP1. Five unique de novo KEAP1 nonsynonymous mutations that suggested loss of function (Supplementary Methods) were found among CDDP-resistant clones derived from HN30 and HN31 (Fig. 1b and Supplementary Table S4), but not PCI13.

To systematically distinguish mutated genes that may have been selected for during acquisition of CDDP resistance, we utilised a novel analysis technique we recently described [36], referred to as cohort integral (CI). The CI technique compares the distribution of pathogenicity scores of the variants in each gene, estimated by the evolutionary action (EA) method [37], with a reference distribution that was generated using the variants of all genes. Therefore, the EA-CI method should detect CDDP resistance driver genes enriched for impactful variants relative to the reference distribution, which mostly consist of passenger variants. Using the EA-CI approach, we identified 18 candidate genes with recurrent (≥3) mutations and EA distributions with a P value less than 0.05, which reduced to 10 mutated genes when further filtered to exclude those with low RNA expression
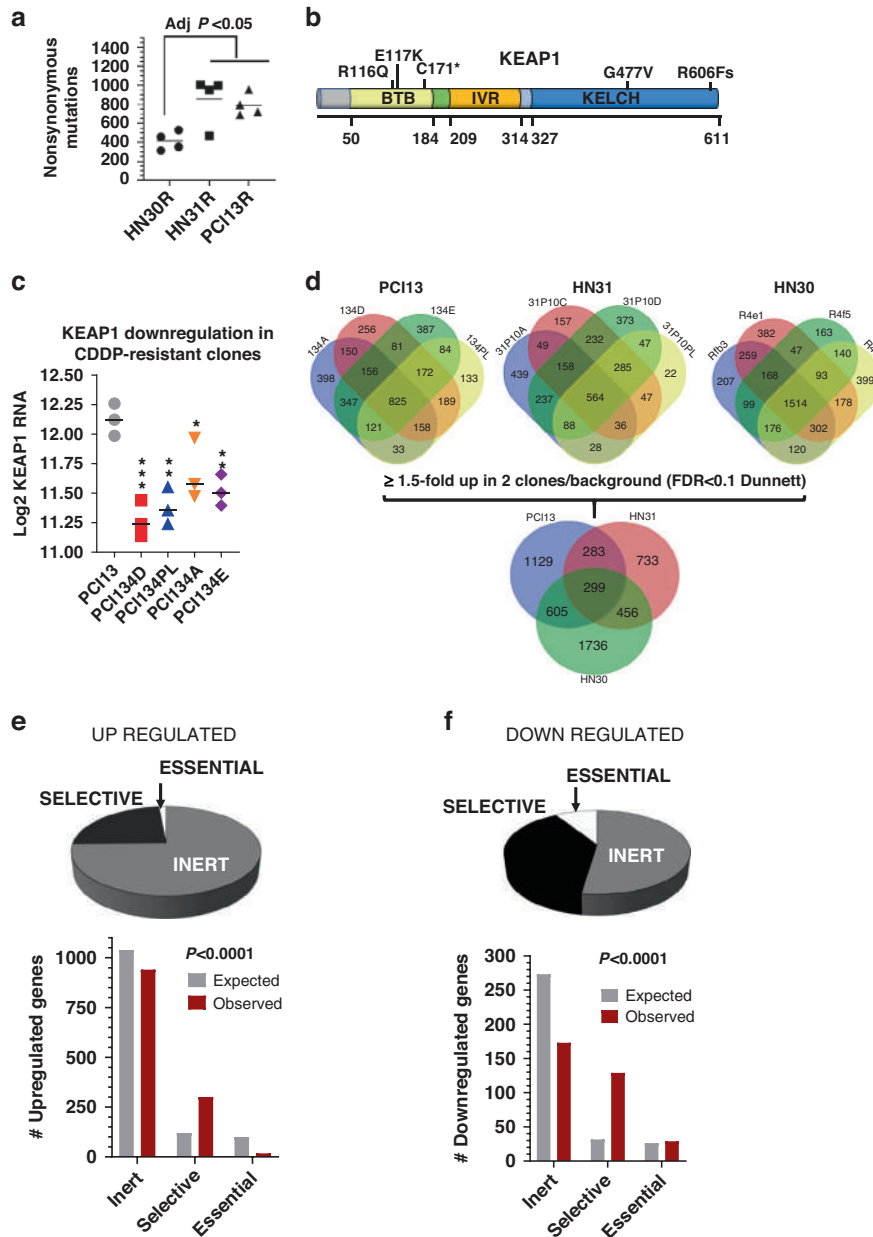
Fig. 1 Mutational and transcriptional shifts associated with CDDP resistance. a Whole-exome mutational analysis of parental and CDDP-resistant (R) clones. **b** Spectrum of KEAP1 mutations in CDDP-resistant clones. **c** KEAP1 mRNA is downregulated in all individual PCI13 CDDP-resistant clones. ***P < 0.001, **P < 0.01, *P < 0.05. **d** Venn diagram of genes upregulated by ≥1.5-fold in CDDP-resistant clones as determined by the Dunnett's multiple comparison test (FDR < 0.1). Distribution of functional classes among genes upregulated (**e**) or downregulated (**f**) in at least two clones from at least two backgrounds. Essential, selective, and inert are defined in the text and observed distribution was compared to the expected distribution with a Chi-square test.

(Supplementary Table S5). As expected, *KEAP1* was among the ten candidate driver genes identified by this method (Supplementary Fig. 2A, *P* < 0.009). In addition, we identified: *EPPK1* (Supplementary Fig. 2A), linked to cell migration, EMT, and the cytoskeleton; *PROSER1*, an epigenetic regulator; and *VPS13A*, involved in protein transport. Since most mutated genes in the resistant clones had less than three variants and were excluded from the gene-level EA-CI analysis, we also performed a pathway-level EA-CI analysis. For this we asked whether multiple genes from individual pathways collectively had a CI indicative of selection, as we showed previously [38]. Pathways were obtained from the Reactome database [39]. Fifteen different pathways, including Adenylate cyclase, mTORC1 signalling, mitochondrial tRNA

aminoacylation, and protein kinase A activation had mutational CI bias consistent with selection during acquired CDDP resistance (Supplementary Table 6 and Supplementary Fig. 2B).

Differential gene expression in CDDP-resistant clones

Whole transcriptome analysis (i.e., RNA-seq) was used to compare gene expression for four different CDDP-resistant clones from each genetic background with their respective drug-naive parental lines. Because PCI13-resistant clones lacked *KEAP1* mutations found in cells derived from HN30 and HN31, we first looked at whether altered *KEAP1* mRNA levels in the former might represent an alternative mechanism for reduced KEAP1 function. Indeed, levels of *KEAP1* mRNA were approximately twofold lower

in CDDP-resistant PCI13 clones compared to their parental cells (Fig. 1c). Globally, we detected hundreds of genes significantly upregulated and downregulated in resistant cells, with many shared genes among individual clones (Fig. 1d, Supplementary Fig. 3 and Supplemental Tables S7 and S8) derived from the same cell line, and 217 genes commonly upregulated in two or more resistant clones from all three parental backgrounds (Fig. 1d). Overall, fewer genes were downregulated in the resistant cell lines and far fewer of these (i.e., 28) were conserved across clones from all three parental backgrounds. To broadly understand the biology of genes differentially expressed, we categorised them as "essential", "selective" or "inert" based on public data (Supplementary Materials and Methods). We then examined genes upregulated or downregulated ≥1.5-fold (in at least two CDDP-resistant clones from two or more parental backgrounds) for their distribution of *essential, selective, or inert* categories (Fig. 1e, f). Most genes upregulated in CDDP-resistant clones (i.e., 75%) were classified as inert, suggesting they may only be critical for proliferation/survival under conditions of stress, like growth in the presence of CDDP. Interestingly, in both the upregulated and downregulated gene lists there was significant enrichment for genes categorised as selective.

Among the 217 commonly upregulated genes across all three genetic backgrounds, we observed a large range of average fold increases, which frequently exceeded 10-fold even for genes with moderate to high expression levels (Supplementary Fig. 5). Included in this group were genes which function in amino acid transport/trafficking, chromatin remodelling, cytoskeleton, adhesion, and catalysis of amine carcinogens. Gene Ontology (GO) enrichment analysis of the 217 commonly upregulated genes identified many different metabolic processes, including xenobiotic response to stress, glucuronidation, regulation of fatty acids, carbohydrates, and monocarboxylic acid (Supplementary Table S9). Although no GO enrichment was found for the common 28 genes downregulated across all three cell backgrounds, expanding the list to genes downregulated in at least two clones from at least two backgrounds (i.e., 351 genes from Supplementary Fig. 3) identified enrichment for processes related to cell death/apoptosis, and nitrogen metabolism (Supplementary Table S10). We further performed an unbiased gene set enrichment analysis (GSEA) of differentially expressed genes using Hallmark pathways defined by the Molecular Signature Database. As shown in Supplemental Table 11, CDDP-resistant clones consistently demonstrated depletion of pathways involved in: proliferation (MYC, E2F, G2M checkpoint), DNA-damage repair, oxidative phosphorylation (OxPhos) and a consistent enrichment of the epithelial-mesenchymal transition pathway.

Transcriptomic analysis reveals activation of the NRF2 pathway, but not DNA-damage response, in CDDP-resistant cells

Since resistance to CDDP may occur due to upregulation of DNA-damage repair pathways, we focused on detecting this phenomenon. A robust gene signature for DNA-damage response (DDR) activation was developed by employing a combination of bioinformatic steps (Supplementary Materials and Methods, and Supplementary Fig. 6). Using this validated DDR signature, we found that CDDP-resistant clones derived from PCI13 had substantially lower DDR gene activation than their drug-naive parental cells ($P < 0.0001$, Supplementary Fig. 7). The majority of CDDP-resistant clones derived from HN30 and HN31 showed no significant differences in DDR gene activation scores from their drug-sensitive parental lines, demonstrating that upregulation of DDR was not associated with the CDDP-resistant phenotype. This was further supported by the observation that *SSRP1*, an essential gene thought critical to regulation of CDDP-induced DNA-damage response (not part of the 69 gene signature) was also found to be significantly

downregulated in 9/12 CDDP-resistant clones (Supplementary Table S8). Overall, this is consistent with a reduced dependence on activation of DNA-damage repair possibly because less CDDP-derived free radicals are able to reach the DNA in the first place and matches our previously published findings in HN30 and its resistant clones showing reduced formation of γH2AX foci in the context of CDDP exposure [9].

We previously derived a robust 138 gene signature of NRF2 activation using similar bioinformatic approaches, which was validated in TCGA cohorts harbouring mutations in either *KEAP1* or *NRF2* [18]. Nrf2 activation measured by ssGSEA scores was significantly higher in 8/12 CDDP-resistant clones derived from all three parental backgrounds (Fig. 2a). Individually, expression of many Nrf2 targets from the signature was elevated in the resistant cell lines (Fig. 2b and Supplementary Table S7), including multiple UDP-glucuronosyltransferases, glutathione peroxidase 2 (GPX2), aldo-keto reductase family 1 members, along with other canonical genes regulated by Nrf2 (e.g., Glutamate-cysteine ligase modifier/GCLM). To contextualise the increased expression of Nrf2 targets in CDDP-resistant clones, we used fold changes to normalise RNA values to an earlier dataset with expression date from a panel of 60 HNSCC cell lines, which also included the drug-naive parental lines (Fig. 2c). Using a subset of 14 genes that were consistently upregulated across all backgrounds and in all clones, we clustered our CDDP-resistant clones against the panel of 60 other parental HNSCC cell lines using normalised values. With one exception, CDDP-resistant clones clustered together, and in proximity with other cell lines containing de novo *KEAP1* mutations (Fig. 2c).

Proteomic alterations associated with CDDP resistance

To determine whether transcriptomic alterations measured in the CDDP-resistant clones are detectable at the protein level, we globally profiled proteins in HN30, HN30R4E1 and HN30R4F5 by mass spectrometry analysis (Supplementary Fig. 8A) and identified 257 proteins commonly upregulated and 224 commonly downregulated among CDDP-resistant clones (Fig. 3 and Supplementary Table S12). Of the 50 genes included in our Nrf2 signature that were detected by the mass spectrometry platform, 19 (38%) were significantly upregulated in both resistant clones, with an additional five upregulated in at least one clone (Supplementary Table S12). No proteins from the Nrf2 signature were downregulated in both clones and only three were downregulated in one clone (Supplementary Table S12). In accordance with inactivating *KEAP1* mutations found in HN30R4E1 and HN30R4F5, no Keap1 protein was detectable by mass spectrometry in either clone despite being abundantly present in CDDP-sensitive parental HN30 (not shown)—albeit we excluded Keap1 and other undetectable proteins from downstream statistical analysis. Globally, we detected a high concordance between proteins differentially regulated in CDDP-resistant clones and changes in their RNA ($P < 0.0001$, Supplementary Table S12). Individual proteins of interest which demonstrated increased levels in both clones compared to the parental cell line included AKRCCs, GGT2 (gamma glutamyltransferase), VAT1 (oxidoreductase), HSPB11 (protein stabilisation), ACOX1 (fatty acid oxidation) and CD109 (serine endopeptidase inhibitor). GO pathway enrichment utilising proteins upregulated in either HN30R4E1 or HN30R4F5 identified many upregulated processes in common (Supplementary Fig. 3A, Supplementary Table S13), including metabolism of oxoacid, glutathione, NADP, glucose 6-phosphate, prostanoids, and processes associated with the pentose phosphate shunt, protein transport, ribosome biogenesis, and detoxification. Integrated analysis of several pathways revealed upregulation at both the protein and RNA levels (Supplementary Fig. 8B), suggesting coordinated regulation of gene transcription and protein translation were contributing to an altered metabolic state. DNA repair and negative regulation of translation were among the top
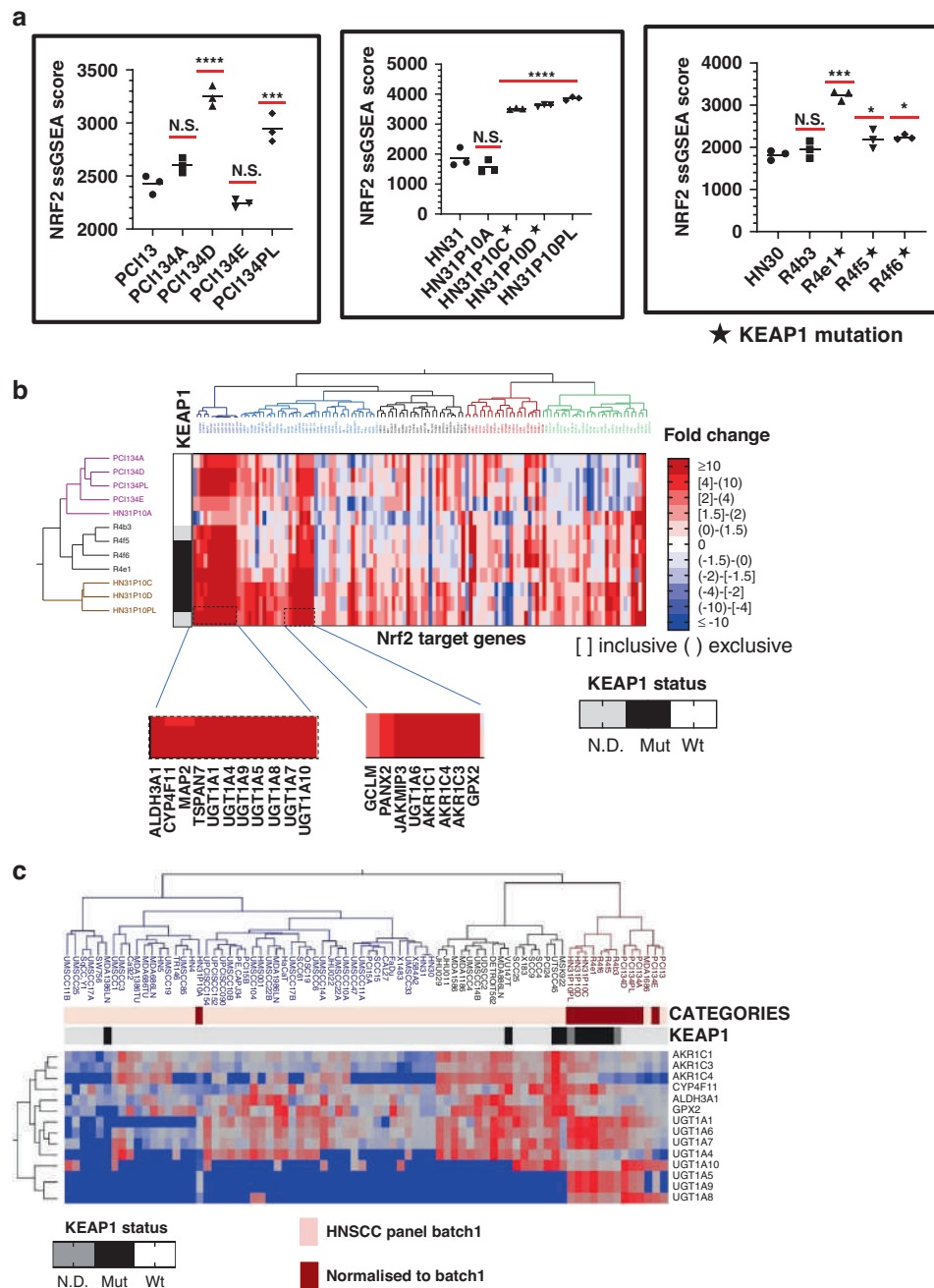
Fig. 2 Activation of Nrf2 in CDDP-resistant clones. a Overall, 8/12 individual clones demonstrated significant increases in the Nrf2 ssGSEA score compared to the parental cell lines. ****Adj*P*<0.0001, ***Adj*P*<0.001, and *Adj*P*<0.05 by Tukey 's Honest Significant Difference test. **b** Ward's hierarchical clustering of individual CDDP-resistant clones by fold changes in RNA expression of Nrf2 downstream target genes used to calculate the Nrf2 ssGSEA scores above. The *KEAP1* mutational status of clones is annotated vertically and Nrf2 target genes with the most consistent and robust upregulation are annotated horizontally across the bottom. **c** RNA expression of the most robustly upregulated Nrf2 target genes from (**b**) in a large panel of established HNSCC cell lines (i.e., batch 1), along with normalised imputed values from the CDDP-resistant clones were used for two-way Ward's clustering to contextualise the degree of overexpression relative to drug-naive cell lines with or without existing *KEAP1* mutations. Fold change in CDDP-resistant clones relative to their parental lines (also appearing in the batch 1 analysis) were used to impute normalised values for clustering and comparison.

pathways associated with proteins downregulated (Fig. 3b and Supplementary Table S14).

We then examined the functional contribution of Nrf2 signalling to CDDP resistance in HN30E1, the HN30-derived clone which demonstrated the most profound increase in the ssGSEA *NRF2* score. The IC$_{50}$ for CDDP in HN30E1 was roughly 10-fold higher in HN30R4E1 compared to parental HN30 (Supplementary Fig. 9A). Knockdown of *NRF2* expression in HN30R4E1 with shRNA reduced

the IC$_{50}$ of the resistant cells by about half in both a short-term assay (Supplementary Fig. 9B), and in a standard clonogenic survival assay (Supplementary Fig. 9D).

Proliferation/survival tradeoffs and drug resistance in CDDP-resistant cells
All resistant cells survived and proliferated in the presence of supra-therapeutic concentrations of CDDP for over 12 months,
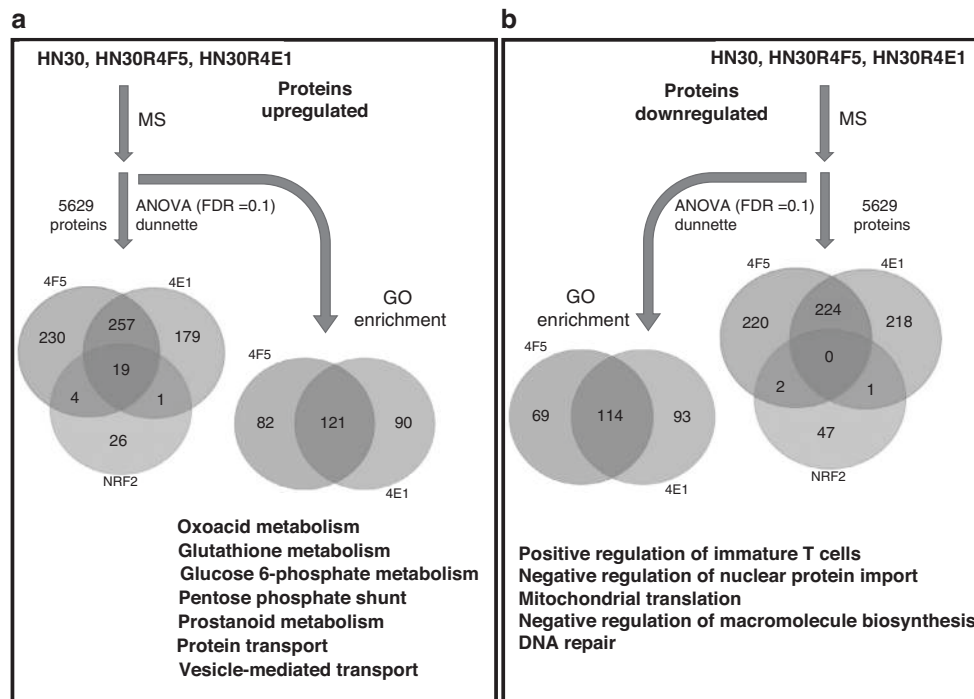
Fig. 3 Protein validation of Nrf2 activation and metabolic reprogramming. Venn diagram of proteins significantly upregulated (**a**) or downregulated (**b**) in CDDP-resistant clones HN30R4F5 or HN30R4E1 relative to parental HN30. Within each panel, the Venn diagram below the double arrows corresponds to the number of proteins altered, with the bottom circle (green) demonstrating overlap among 50 Nrf2 downstream targets that happen to be detected by mass spectrometry. Venn diagrams beneath the curved arrow correspond to the number of GO pathways enriched among proteins altered in each clone. Among proteins contained within the Nrf2 signature, 19 were upregulated in both clones and none were downregulated in both clones. GO analysis revealed multiple significantly enriched and depleted pathways.

with normal nuclear and other organelle integrity as ascertained using TEM (Supplementary Figs. 10A, 11). However, the CDDP-resistant lines did have a greater preponderance of lamellar bodies (Supplementary Fig. 11). Under CDDP-free conditions, resistant clones demonstrate reduced rates of proliferation compared to the parental cell line (Supplementary Figs. 10B and 12) but maintain dependence on extracellular glucose (Glc) for survival/proliferation compared to glutamine (GLN) (Supplementary Fig. 10C–E) similar to the predominant HNSCC metabolic phenotype we defined over a decade ago [40].

To determine whether the acquisition of CDDP resistance is a function of non-specific development of multi-drug resistance (MDR) we performed two independent drug screens. We first compared HN30 to pooled resistant populations (Supplementary Table S15 and Supplementary Fig. 13). GR_{50} values could be calculated for 88 compounds distributed widely across drug classes, targets, and mechanism of anti-cancer activity. Two notable observations were made. First, we did not detect cross-resistance to DNA damaging or other genotoxic agents among the tested compounds in parallel with the known CDDP resistance; this was further validated in two individual compounds using clonogenic survival assays (Supplementary Fig. 13B, F). Second, we did observe a trend toward cross-resistance with proteotoxic agents, which was reproducible in a second screen comparing two individual PCI13 CDDP-resistant clones to the parental cell line (Supplementary Table S16). Since the initial screens generated GR_{50} values based on a limited dose range, we conducted a secondary more detailed analysis for a broader range of doses in two HN30 and 2 PCI13 clones and confirmed a moderate cross-resistance to proteotoxic drugs in the resistant cells as shown in Supplementary Table S17.

Enhanced reductive state and reduced conventional energetic flux in CDDP-resistant cells

Combining our previous findings that some HNSCC cells focus on enhancing reductive potential in response to oxidative stress with the drug screening data led us to hypothesise this may represent a fundamental shift away from energy generation toward biomass synthesis and sought to determine whether this is a universal phenotype regardless of genomic background using several overlapping approaches. Using an individual cell analysis based on autofluorescence lifetime imaging of NAD(P)H and FAD, we found higher NAD(P)H intensities and lower FAD intensities in CDDP-resistant HN30R4E1 cells compared to their corresponding parental cell line (i.e., a decreased redox ratio [FAD/[FAD + NAD(P)H]), suggesting an increased reductive potential of the CDDP-resistant cells (Fig. 4 and Supplementary Fig. 14). In addition, both the free and protein-bound NAD(P)H lifetimes (τ_1 and τ_2) were increased in the CDDP-resistant cells, indicating alterations in the environments of free and bound NAD(P)H (Fig. 4). Changes in the lifetime of bound NAD(P)H, τ_2, suggest alterations in NAD(P)H binding partners and a shift in metabolic pathways. In addition, we found significant reductions in the fraction of bound FAD (α_1; Supplementary Fig. 15) in the CDDP-resistant cells indicating a reduction in mitochondrial metabolism and OxPhos. We validated this altered metabolism in six CDDP-resistant clones from all three cell backgrounds using biochemical measurements of the NADH/NAD + ratio and confirmed an enhanced reductive state (Fig. 4). CDDP-resistant clones had higher baseline levels of both total glutathione (GS) measured biochemically, and reduced glutathione (GSH) measured via fluorescence (Fig. 4).

HNSCC cells are highly dependent on glucose metabolism for biomass and energy production, and though flux through LDH from pyruvate into lactate is high for most lines, there is significant, measurable oxidative phosphorylation (OxPhos)
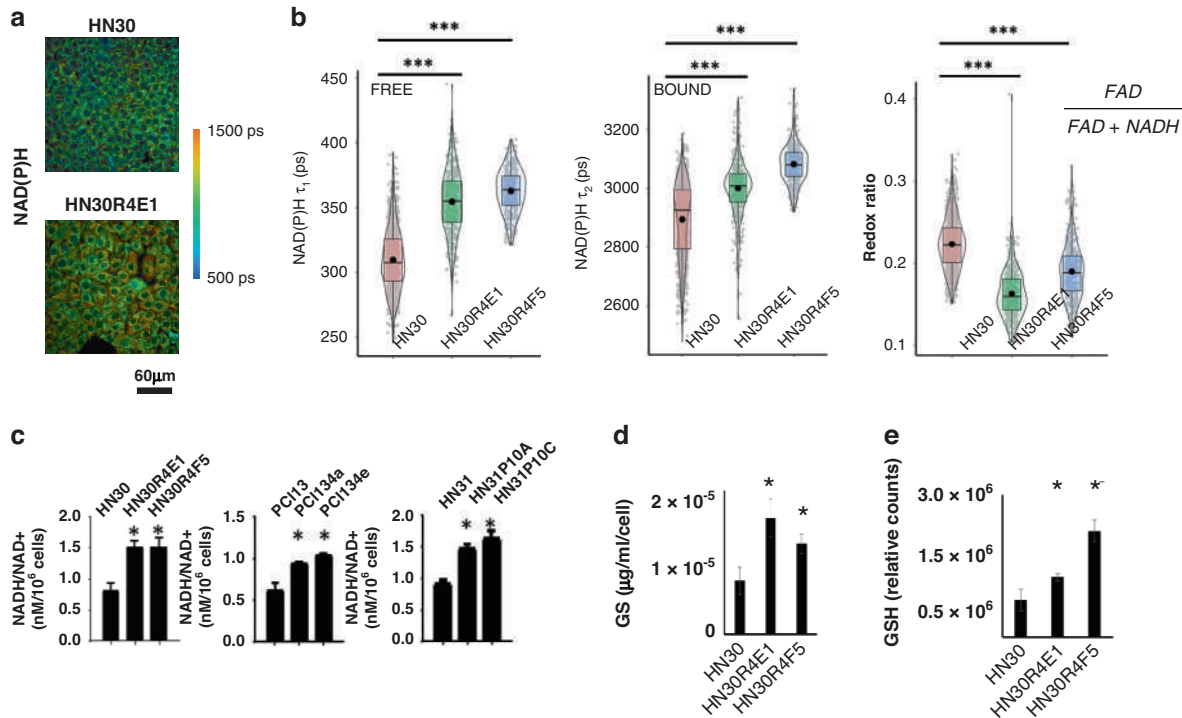
Fig. 4 CDDP-resistant cells have an enhanced reductive potential. CDDP-resistant cells demonstrated increased fluorescence lifetime of NAD(P)H at an individual cell level (scale bar = 60 μm) (**a**) which is due to increased lifetimes of both free and protein-bound (or adjacent) NAD(P)H with a concomitant reduction in the REDOX ratio of FAD/(FAD + NAD(P)H) (**b**). Biochemical measurements confirm a significant increase in the ratio of NADH/NAD + in all three cell lineages under normal growth conditions. Total glutathione (GS) measured biochemically and normalised to cell number (**d**) is significantly higher in CDDP-resistant clones as is reduced glutathione (GSH) measured using fluorescence (**e**). (*$P < 0.05$; **$P < 0.01$; ***$P < 0.001$). Data for (**c–e**) are presented as means + /− standard error of the mean.

detectable under baseline and stress conditions [40]. Four lines of evidence indicate that CDDP-resistant cells re-wire metabolism toward an anabolic state. First, as shown in Fig. 5, LDH activity is reduced by between 20% (PCI13 clones) and 50% (HN30, HN31 clones) in resistant cells compared to parental controls. Second, despite unaltered mitochondrial morphology (TEM) and no evidence of organelle depletion (conventional immunofluorescence; Fig. 5c and quantification), CDDP-resistant clones demonstrate a significant reduction in OxPhos as demonstrated by a >50% reduction in spare respiratory capacity, and a >50% reduction in OxPhos dependent ATP production (Fig. 5 and Supplemental Fig. 17). To determine whether this represents a fundamental alteration of the mitochondrial TCA machinery, we measured the reductive potential of parental and CDDP-resistant cells in the presence of multiple metabolic substrates that require varying combinations of TCA enzymes to generate reducing equivalents. We found that CDDP-resistant clones maintained a similar, and in some cases enhanced reductive potential (Supplemental Fig. 18), making it unlikely that the metabolic shifts related to increased NAD(P)H, diminished LDH, and decreased OxPhos activity were caused by intrinsic defects in mitochondrial function.

Metabolic adaptation to CDDP resistance

GO analysis of transcriptomic shifts accompanying CDDP resistance demonstrated a profound upregulation of detoxification processes (Supplemental Tables 9 and 10). Steady-state metabolomics analysis identified significant increases in amino acid and fatty acid intermediate metabolites across the CDDP-resistant clones along with depletion of TCA, glycolytic and PPP intermediates including metabolites indicative of oxidative stress response (e.g., involved in cysteine synthesis) such as methyl histidine and s-methyl-5-thioadenosine along with depletion of Ser a critical component of glutathione synthesis (Supplemental

Table 18). De novo synthesis of Gly, Ala and Asp was variable when comparing HN30 to its CDDP-resistant clones E1 and F5, although both clones demonstrated increased incorporation of ^{13}C from all ^{13}C-labelled glucose (GLC) into Asp (m + 1 and m + 2) with total and unlabelled Asp levels significantly higher only in the F5 clone (Supplemental Fig. 19). In contrast, both CDDP-resistant clones demonstrated a dramatic increase in total Ser, along with significant higher incorporation of ^{13}C from GLC into Ser (m + 1, m + 2) (Fig. 6). To determine whether this shunting into Ser was indicative of increased de novo production of reducing equivalents, we analysed incorporation of ^{13}C from the two principal sources previously defined in the literature into reduced glutathione (GSH). As shown in Fig. 6, CDDP-resistant cells demonstrated coordinated and significantly higher incorporation of ^{13}C from both Gln (m + 1, m + 9, m + 10) and GLC (m + 1, m + 2, m + 3, m + 4).

DISCUSSION

Introduced into clinical practice in the 1970s, CDDP remains essential in the setting of advanced-stage HNSCC in order to decrease locoregional recurrence and reduce the risk of distant metastasis [1, 6]. Despite its importance, our understanding of how CDDP is processed within tumours and factors which drive resistance remain unclear. Although multiple individual genes and proteins have been linked to intrinsic or acquired CDDP resistance, we have neither an accurate metric to predict CDDP sensitivity or resistance nor effective means to improve response to this drug. Previously, we developed a biochemical model that may explain how tumours respond or adapt to genotoxic therapies like CDDP. Reactive oxygen species (ROS) generated by CDDP or radiation can be absorbed by primary reducing equivalents (e.g., glutathione), with the latter subsequently regenerated using secondary reducing
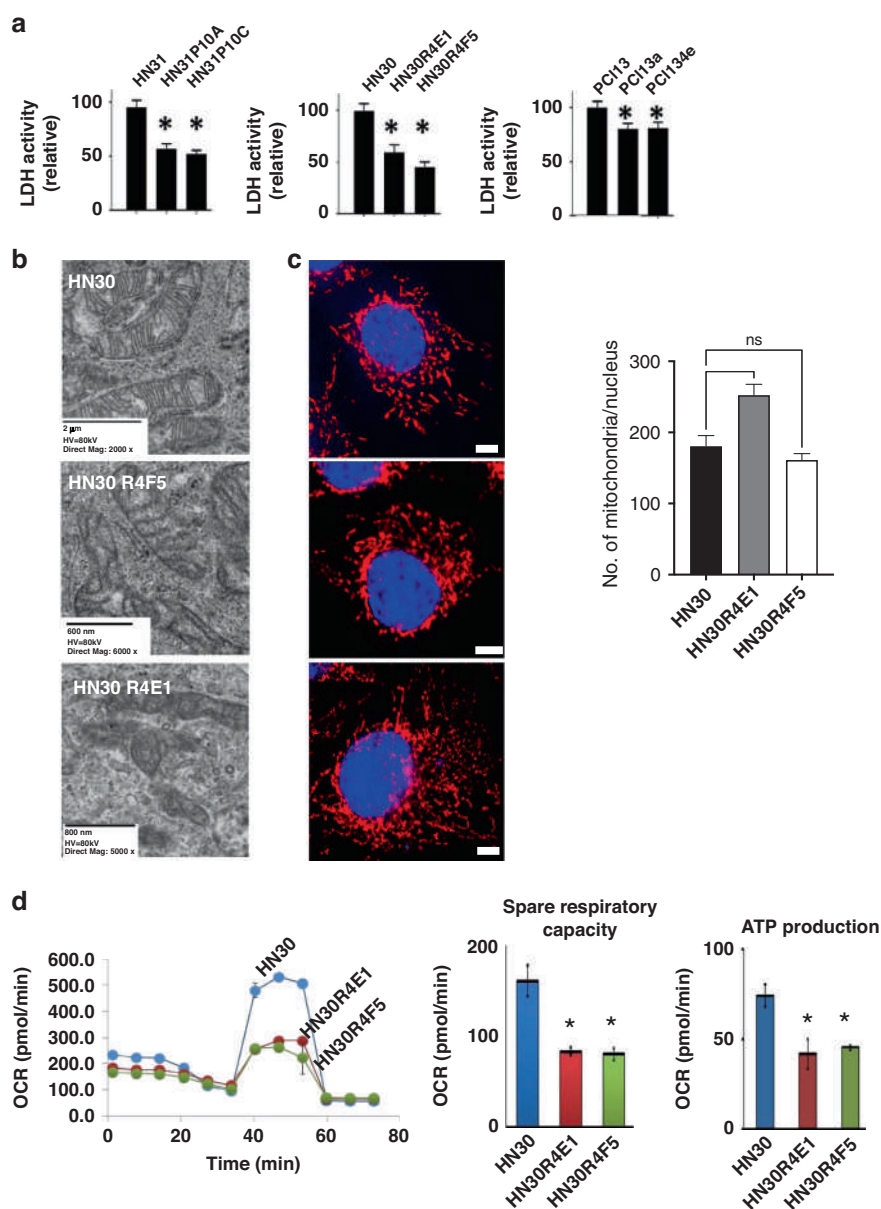
Fig. 5 CDDP-resistant cells have reduced energy production. a Biochemical measurements of lactate dehydrogenase (LDH) activity demonstrated a 20–50% reduction in activity in CDDP-resistant clones compared to parental cell lines (data presented as means with $+/-$ standard error of the mean). **b** No alterations in mitochondrial integrity, morphology or number were detected in CDDP-resistant clones. **c** Representative fluorescence images of cells stained with MitoTracker and DAPI, with quantified mitochondria number per nucleus. Data are represented as the mean $\pm$ SEM ($n > =3$, at least 50 cells per experiment). Scale bar is 10 μm. Red fluorescence, mitochondria; blue fluorescence, DAPI-labelled nucleus. **d** Despite this HN30R4E1 and HN30R4F5 both demonstrated a ~50% reduction in spare respiratory capacity and oxidative phosphorylation-dependent ATP production compared to HN30 (measured using Seahorse; OCR = oxygen consumption rate; data normalised to cell number; data presented as means with $+/-$ standard deviation). ($*P < 0.05$; $**P < 0.01$; $***P < 0.001$).

equivalents (NADH, NADPH) [8, 9, 14, 19, 41–45]. Depletion of NADH pools forces cells to "borrow" NADH from normal reductive carbon (C) reactions, such as the conversion of pyruvate into lactate by lactate dehydrogenase (LDH), resulting in decreased C-flux through these reactions. We have published experimental evidence supporting this model using biochemical measurements of LDH activity, ^{13}C-flux mass spectrometry measurements (MS) and magnetic resonance spectroscopic imaging of hyper-polarised ^{13}C-pyruvate (HP-MRI) [8, 9, 14, 19, 41–45]. We have confirmed the link between genotoxic therapy and shifts in the cellular reductive state or C-flux under both in vitro and in vivo conditions in multiple preclinical tumour models, including HNSCC and anaplastic thyroid carcinoma (ATC) [8, 9, 14, 19, 41–45]. In this study, we sought to determine first,

whether this "borrower" metabolic phenotype is imprinted in HNSCC cells with acquired CDDP resistance and second, how cells enact and support this phenotype at a genomic and transcriptomic level.

Despite data from other tumour types, acquired resistance in our HNSCC models does not seem to involve upregulation of DNA-damage repair (DDR) pathways. We previously showed the CDDP-resistant cells require much higher doses of CDDP to activate DDR in the form of γH2ax foci [9] and trigger senescence in the HN30 background; this is accompanied by a decreased sensitivity of wild-type *TP53* to CDDP-generated stress and reduced binding of CDDP to DNA. At both mRNA and protein levels, we detect absolutely no evidence of enhanced DDR in
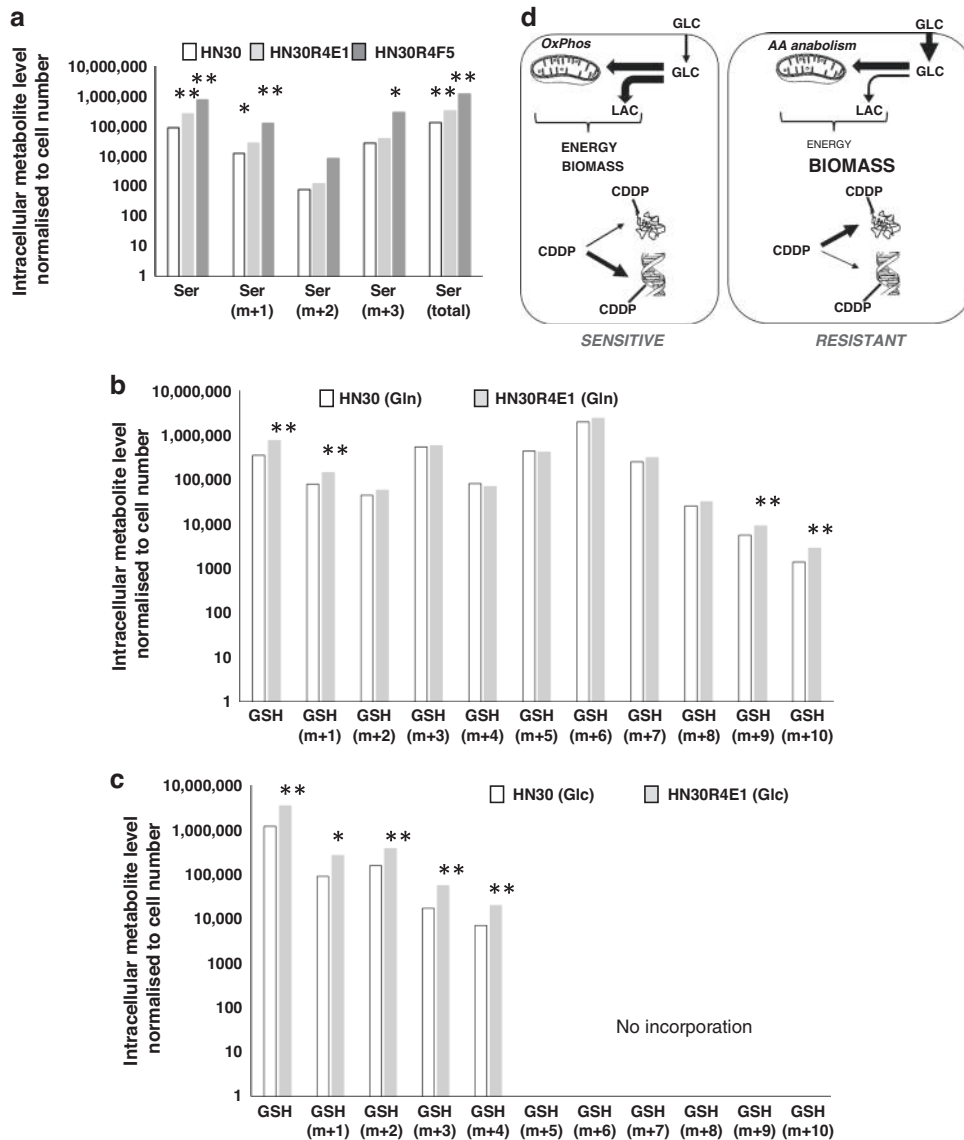
Fig. 6 Differential carbon flux in CDDP-resistant clones. a Under normal growth conditions, there is increased ^{13}C incorporation from 15 mM all carbon ^{13}C-labelled glucose (GLC) in CDDP-resistant clones into serine (Ser) (48 h). **b** Overall, ^{13}C from GLC is incorporated to a greater degree in HN30R4E1 compared to HN30 as is ^{13}C from Gln (**c**). m + x denotes ^{13}C labelling of x carbon atoms. (*$P < 0.05$; **$P < 0.01$; ***$P < 0.001$). **d** Conceptual summary of increased biomass generation designed to absorb CDDP-generated stress in CDDP-resistant cells, preventing DNA binding and damage.

CDDP-resistant cells regardless of parental background, *RAS* or *TP53* mutational status. In fact, DDR gene expression is reduced in PCI13-resistant clones and DDR-related proteins are among proteins with decreased levels in HN30-resistant clones. Based on our previous phenotypic data [9], extended here to two other cellular backgrounds at a genomic, transcriptomic, and proteomic level, our results do not support an essential role for enhanced DDR in the context of acquired CDDP resistance for HNSCC.

Instead, our data from multiple platforms strongly suggests an increased intracellular reductive state which simply prevents CDDP from ever reaching the DNA in the first place. Here, we provide several lines of evidence for this enhanced reductive state. First, in three genomic backgrounds, acquired CDDP resistance is accompanied by a substantial upregulation of Nrf2-modulated genes. Interestingly, in HN30 and HN31 which share a patient lineage, this appears to occur in large part through selection and enrichment of cells with *KEAP1* mutations resulting in enhanced Nrf2 signalling. In contrast, in the PCI13 background, where

mutations cannot be detected, the effect is transcriptional, with suppression of *KEAP1* mRNA levels. In all cases however, activation of Nrf2-dependent genes can be consistently measured and validated at a protein level. Molecular suppression of Nrf2 via shRNA partially reverses the acquired CDDP resistance phenotype, functionally linking Nrf2 pathway activation to resistance.

Second, CDDP-resistant cells demonstrate an increased REDOX state with higher levels of reduced NAD(P)H, an increased biosynthetic capacity for total glutathione and higher levels of reduced glutathione under normal growth conditions. This enhanced reductive state appears to represent a trade-off of biomass and energy, as it is accompanied by a dramatic reduction in both LDH and OxPhos activity. In the context of normal mitochondrial morphology, similar overall mitochondrial biomass and retained ability to engage in REDOX activity when semi-permeabilized, these findings strongly suggest that CDDP-resistant cells engage in differential metabolic activity not because mitochondria are defective or absent, but most likely to fulfil

different biomass requirements. This is further supported by transcriptomic and proteomic enrichment of biomass-generating pathways, increases in steady-state intermediates involved in fatty acid and protein synthesis and carbon flux. Third, at a phenotypic level, CDDP-resistant cells appear to trade off proliferation for survival. Although both Gln and GLC requirements are consistent across CDDP-sensitive parental cell lines and their resistant clones, the CDDP-resistant clones demonstrate increased flux from GLC into Ser, a precursor to glutathione (via cysteine) and both sources of carbon (Gln and GLC) are utilised at a higher rate by CDDP-resistant clones. Evidence of this adaptive metabolic rewiring is apparent at both the RNA and protein level, where changes were observed in glucose and glutathione metabolism as well as the pentose phosphate shunt pathway.

Taken together, these data support an imprinted "borrower" phenotype whereby acquisition of CDDP resistance is accompanied by a metabolic shift away from normal energy and biomass toward a phenotype dominated by biomass generation for the purposes of CDDP absorption and disposal (Fig. 6d), preventing DNA damage and activation of cell death cascades. What does this mean for translational applications? First, the fact that across different backgrounds, the phenotype converges on upregulation of Nrf2 signalling strongly suggests that this is a required step in the adaptation process. Which component(s) of Nrf2 signalling are required remains to be determined, but our data suggest it is likely the primary enzymes involved in glutathione synthesis and recycling. Given the evidence of enhanced C-flux from both GLC and Gln sources and the essentiality of GSH enzymes, it is likely an intermediate downstream step/dependency will need to be targeted to attack this potential vulnerability while avoiding significant solid organ toxicity [3, 5, 46–48]. Second, a consistent metabolic shift suggests the potential for biomarker development is real. We have shown that HP-MRI/MRS of C conversions such as the pyruvate → lactate conversion can detect both acute and chronic shifts in metabolic activity reflective of differential reductive states [14, 19, 41–45]. If in fact the "borrower" phenotype is imprinted in CDDP-resistant cells and tumours, it suggests that HP-MRI/MRS could act as a real-time biomarker of response or resistance during the treatment of HNSCC. Whether this can be operationalized will depend heavily on planned validation experiments in both patient-derived xenograft (PDX) models and human tumours from patients undergoing CDDP-based treatment.

In addition to the absence of DDR upregulation, one additional noteworthy negative finding requires mention. With the exception of a moderate increase in resistance to proteotoxic agents, there is simply no clear evidence of multi-drug resistance (MDR) in our HNSCC model. This contradicts previous findings and calls into question the impact of non-specific resistance mediators such as p-glycoprotein. Nevertheless, this finding is encouraging for it suggests conventional and/or targeted agents that do not function through ROS generation may in fact remain effective.

One potential caveat of the present work is that selection for CDDP resistance was performed in vitro with cell lines. However, we have now have a compendium of parallel in vivo analyses using our CDDP-resistant cells that confirms they remain refractory to CDDP treatment and maintain an elevated Nrf2 signature when grown orthotopically in mice, but can be rendered sensitive by knocking down NRF2 or restoring a wild-type KEAP1 gene [49]. Furthermore, activation of the Nrf2 pathway through somatic mutations in KEAP1 or transcriptional regulation are unlikely to be artifacts of cell culture as alterations in NRF2/KEAP1 are well documented in primary untreated tumours, including HNSCC, where they are recognised to be cancer drivers. We recently demonstrated elevated Nrf2 activity in a substantial subset of primary untreated tumours derived from the lung, bladder, and head and neck using the TCGA transcriptomic data [18]. Our current analysis identified a trend towards reduced survival among TCGA head and neck cancer patients whose tumours had elevated Nrf2 signatures, when treated with CDDP (Supplemental Fig. 20). Because the multiple KEAP1 mutations we found in our CDDP-resistant clones lacked the same CDDP mutagenic signature observed with many of the other somatic mutations, it is possible they were pre-existing at a low frequency (as has been observed with drug resistance in many other systems) and were selected for during the stress of CDDP exposure. This raises the possibility that the distinction between acquired and innate CDDP resistance could be a function of the degree to which elevated tumours with Nrf2 activation exist in a primary tumour and could explain why we found decreased survival in head and neck cancer patients treated with CDDP when their pretreated tumours had elevated Nrf2 signatures. Our findings warrant future studies to examine whether pre-existing NRF2/KEAP1 pathway mutations or an elevated transcriptomic Nrf2 signature can predict CDDP failure in patients and patient derived xenograft (PDX) models.

DATA AVAILABILITY
The data generated in this study are available within the article and its supplementary data files.

REFERENCES

1. Bauml JM, Vinnakota R, Anna Park YH, Bates SE, Fojo T, Aggarwal C, et al. Cisplatin every 3 weeks versus weekly with definitive concurrent radiotherapy for squamous cell carcinoma of the head and neck. J Natl Cancer Inst. 2019;111:490–7.
2. Cepeda V, Fuertes MA, Castilla J, Alonso C, Quevedo C, Perez JM. Biochemical mechanisms of cisplatin cytotoxicity. Anticancer Agents Med Chem. 2007;7:3–18.
3. Chen HH, Song IS, Hossain A, Choi MK, Yamane Y, Liang ZD, et al. Elevated glutathione levels confer cellular sensitization to cisplatin toxicity by up-regulation of copper transporter hCtr1. Mol Pharm. 2008;74:697–704.
4. Drayton RM, Catto JW. Molecular mechanisms of cisplatin resistance in bladder cancer. Expert Rev Anticancer Ther. 2012;12:271–81.
5. Du H, Chen B, Jiao NL, Liu YH, Sun SY, Zhang YW. Elevated glutathione peroxidase 2 expression promotes cisplatin resistance in lung adenocarcinoma. Oxid Med Cell Longev. 2020;2020:7370157.
6. Mehanna H, Robinson M, Hartley A, Kong A, Foran B, Fulton-Lieuw T, et al. Radiotherapy plus cisplatin or cetuximab in low-risk human papillomavirus-positive oropharyngeal cancer (De-ESCALaTE HPV): an open-label randomised controlled phase 3 trial. Lancet. 2019;393:51–60.
7. Mezencev R, Matyunina LV, Wagner GT, McDonald JF. Acquired resistance of pancreatic cancer cells to cisplatin is multifactorial with cell context-dependent involvement of resistance genes. Cancer Gene Ther. 2016;23:446–53.
8. Yu W, Chen Y, Dubrulle J, Stossi F, Putluri V, Sreekumar A, et al. Cisplatin generates oxidative stress which is accompanied by rapid shifts in central carbon metabolism. Sci Rep. 2018;8:4306.
9. Yu W, Chen Y, Putluri N, Coarfa C, Robertson MJ, Putluri V, et al. Acquisition of cisplatin resistance shifts head and neck squamous cell carcinoma metabolism toward neutralization of oxidative stress. Cancers. 2020;12:1670.
10. Zhu H, Luo H, Zhang W, Shen Z, Hu X, Zhu X. Molecular mechanisms of cisplatin resistance in cervical cancer. Drug Des Dev Ther. 2016;10:1885–95.
11. Galluzzi L, Senovilla L, Vitale I, Michels J, Martins I, Kepp O, et al. Molecular mechanisms of cisplatin resistance. Oncogene. 2012;31:1869–83.
12. Makovec T. Cisplatin and beyond: molecular mechanisms of action and drug resistance development in cancer chemotherapy. Radio Oncol. 2019;53:148–58.
13. Pham D, Deter CJ, Reinard MC, Gibson GA, Kiselyov K, Yu W, et al. Using ligand-accelerated catalysis to repurpose fluorogenic reactions for platinum or copper. ACS Cent Sci. 2020;6:1772–88.
14. Sandulache VC, Chen Y, Feng L, William WN, Skinner HD, Myers JN, et al. Metabolic interrogation as a tool to optimize chemotherapeutic regimens. Oncotarget. 2017;8:18154–65.
15. Niehr F, Eder T, Pilz T, Konschak R, Treue D, Klauschen F, et al. Multilayered omics-based analysis of a head and neck cancer model of cisplatin resistance reveals intratumoral heterogeneity and treatment-induced clonal selection. Clin Cancer Res. 2018;24:158–68.
16. Simons AL, Ahmad IM, Mattson DM, Dornfeld KJ, Spitz DR. 2-Deoxy-D-glucose combined with cisplatin enhances cytotoxicity via metabolic oxidative stress in human head and neck cancer cells. Cancer Res. 2007;67:3364–70.

17. Krupar R, Hautmann MG, Pathak RR, Varier I, McLaren C, Gaag D, et al. Immunometabolic determinants of chemoradiotherapy response and survival in head and neck squamous cell carcinoma. Am J Pathol. 2018;188:72–83.

18. Kazi MA, Veeramachaneni R, Deng D, Putluri N, Cardinas M, Sikora A, et al. Glutathione peroxidase 2 is a metabolic driver of the tumor immune microenvironment and immune checkpoint inhibitor response. J ImmunoTher Cancer. 2022;10:e004752.

19. Sandulache VC, Chen Y, Skinner HD, Lu T, Feng L, Court LE, et al. Acute tumor lactate perturbations as a biomarker of genotoxic stress: development of a biochemical model. Mol Cancer Ther. 2015;14:2901–8.

20. Zhao M, Sano D, Pickering CR, Jasser SA, Henderson YC, Clayman GL, et al. Assembly and initial characterization of a panel of 85 genomically validated cell lines from diverse head and neck tumor sites. Clin Cancer Res. 2011; https://doi.org/10.1158/1078-0432.CCR-11-0690.

21. Frederick M, Skinner HD, Kazi SA, Sikora AG, Sandulache VC. High expression of oxidative phosphorylation genes predicts improved survival in squamous cell carcinomas of the head and neck and lung. Sci Rep. 2020;10:6380.

22. Wu M, Neilson A, Swift AL, Moran R, Tamagnine J, Parslow D, et al. Multiparameter metabolic analysis reveals a close link between attenuated mitochondrial bioenergetic function and enhanced glycolysis dependency in human tumor cells. Am J Physiol Cell Physiol. 2007;292:C125–36.

23. Alhallak K, Rebello LG, Muldoon TJ, Quinn KP, Rajaram N. Optical redox ratio identifies metastatic potential-dependent changes in breast cancer cell metabolism. Biomed Opt Express. 2016;7:4364–74.

24. Chance B, Schoener B, Oshino R, Itshak F, Nakase Y. Oxidation-reduction ratio studies of mitochondria in freeze-trapped samples. NADH and flavoprotein fluorescence signals. J Biol Chem. 1979;254:4764–71.

25. Hou J, Wright HJ, Chan N, Tran R, Razorenova OV, Potma EO, et al. Correlating two-photon excited fluorescence imaging of breast cancer cellular redox state with seahorse flux analysis of normalized cellular oxygen consumption. J Biomed Opt. 2016;21:60503.

26. Kolenc OI, Quinn KP. Evaluating cell metabolism through autofluorescence imaging of NAD(P)H and FAD. Antioxid Redox Signal. 2019;30:875–89.

27. Lakowicz JR, Szmacinski H, Nowaczyk K, Johnson ML. Fluorescence lifetime imaging of free and protein-bound NADH. Proc Natl Acad Sci USA. 1992;89:1271–5.

28. Varone A, Xylas J, Quinn KP, Pouli D, Sridharan G, McLaughlin-Drubin ME, et al. Endogenous two-photon fluorescence imaging elucidates metabolic changes related to enhanced glycolysis and glutamine consumption in precancerous epithelial tissues. Cancer Res. 2014;74:3067–75.

29. Walsh AJ, Cook RS, Manning HC, Hicks DJ, Lafontant A, Arteaga CL, et al. Optical metabolic imaging identifies glycolytic levels, subtypes, and early-treatment response in breast cancer. Cancer Res. 2013;73:6164–74.

30. Walsh AJ, Mueller KP, Tweed K, Jones I, Walsh CM, Piscopo NJ, et al. Classification of T-cell activation via autofluorescence lifetime imaging. Nat Biomed Eng. 2021;5:77–88.

31. Nakashima N, Yoshihara K, Tanaka F, Yagi K. Picosecond fluorescence lifetime of the coenzyme of D-amino acid oxidase. J Biol Chem. 1980;255:5261–63.

32. Walsh AJ, Skala MC. An automated image processing routine for segmentation of cell cytoplasms in high-resolution autofluorescence images. Proc. SPIE. 2014;8948:161–6.

33. Henderson YC, Mohamed ASR, Maniakas A, Chen Y, Powell RT, Peng S, et al. A high-throughput approach to identify effective systemic agents for the treatment of anaplastic thyroid carcinoma. J Clin Endocrinol Metab. 2021;106:2962–78.

34. Osman AA, Neskey DM, Katsonis P, Patel AA, Ward AM, Hsu TK, et al. Evolutionary action score of TP53 coding variants is predictive of platinum response in head and neck cancer patients. Cancer Res. 2015;75:1205–15.

35. Boot A, Huang MN, Ng AWT, Ho SC, Lim JQ, Kawakami Y, et al. In-depth characterization of the cisplatin mutational signature in human cell lines and in esophageal and liver tumors. Genome Res. 2018;28:654–65.

36. Hsu TK, Asmussen J, Koire A, Choi BK, Gadhikar MA, Huh E, et al. A general calculus of fitness landscapes finds genes under selection in cancers. Genome Res. 2022;32:916–29.

37. Katsonis P, Lichtarge O. A formal perturbation equation between genotype and phenotype determines the evolutionary action of protein-coding variations on fitness. Genome Res. 2014;24:2050–8.

38. Koire A, Katsonis P, Kim YW, Buchovecky C, Wilson SJ, Lichtarge O. A method to delineate de novo missense variants across pathways prioritizes genes linked to autism. Sci Transl Med. 2021;13:eabc1739.

39. Gillespie M, Jassal B, Stephan R, Milacic M, Rothfels K, Senff-Ribeiro A, et al. The reactome pathway knowledgebase 2022. Nucleic Acids Res. 2022;50:D687–92.

40. Sandulache VC, Ow TJ, Pickering CR, Frederick MJ, Zhou G, Fokt I, et al. Glucose, not glutamine, is the dominant energy source required for proliferation and survival of head and neck squamous carcinoma cells. Cancer. 2011;117:2926–38.

41. Sandulache VC, Skinner HD, Wang Y, Chen Y, Dodge CT, Ow TJ, et al. Glycolytic inhibition alters anaplastic thyroid carcinoma tumor metabolism and improves response to conventional chemotherapy and radiation. Mol Cancer Ther. 2012;11:1373–80.

42. Ramirez MS, Lee J, Walker CM, Sandulache VC, Hennel F, Lai SY, et al. Radial spectroscopic MRI of hyperpolarized [1-(13) C] pyruvate at 7 tesla. Magn Reson Med. 2014;72:986–95.

43. Sandulache VC, Chen Y, Lee J, Rubinstein A, Ramirez MS, Skinner HD, et al. Evaluation of hyperpolarized [1-(1)(3)C]-pyruvate by magnetic resonance to detect ionizing radiation effects in real time. PLoS ONE. 2014;9:e87031.

44. Bankson JA, Walker CM, Ramirez MS, Stefan W, Fuentes D, Merritt ME, et al. Kinetic modeling and constrained reconstruction of hyperpolarized [1-13C]-pyruvate offers improved metabolic imaging of tumors. Cancer Res. 2015;75:4708–17.

45. Lee J, Ramirez MS, Walker CM, Chen Y, Yi S, Sandulache VC, et al. High-throughput hyperpolarized (13)C metabolic investigations using a multi-channel acquisition system. J Magn Reson. 2015;260:20–7.

46. Simons AL, Parsons AD, Foster KA, Orcutt KP, Fath MA, Spitz DR. Inhibition of glutathione and thioredoxin metabolism enhances sensitivity to perifosine in head and neck cancer cells. J Oncol. 2009;2009:519563.

47. Dannenmann B, Lehle S, Hildebrand DG, Kubler A, Grondona P, Schmid V, et al. High glutathione and glutathione peroxidase-2 levels mediate cell-type-specific DNA damage protection in human induced pluripotent stem cells. Stem Cell Rep. 2015;4:886–98.

48. Brigelius-Flohe R, Maiorino M. Glutathione peroxidases. Biochimica et Biophysica Acta. 2013;1830:3289–303.

49. Osman AA, Arslan E, Bartels M, Michikawa C, Lindemann A, Tomczak K, et al. Dysregulation and epigenetic reprogramming of NRF2 signaling axis promote acquisition of cisplatin resistance and metastasis in head and neck squamous cell carcinoma. Clin Cancer Res. 2023; https://doi.org/10.1158/1078-0432.CCR-22-2747.

AUTHOR CONTRIBUTIONS

FUNDING

COMPETING INTERESTS

ETHICS APPROVAL AND CONSENT TO PARTICIPATE

No human subjects were involved in this research; therefore, no ethical approval and consent were required for the research.

CONSENT FOR PUBLICATION

Not applicable.

ADDITIONAL INFORMATION

Supplementary information The online version contains supplementary material available at https://doi.org/10.1038/s41416-023-02253-7.

Correspondence and requests for materials should be addressed to Mitchell J. Frederick or Vlad C. Sandulache.

Reprints and permission information is available at http://www.nature.com/reprints